Mouse mtDNA mutant model of Leber hereditary optic neuropathy

Chun Shi Lin[a,b,1], Mark S. Sharpley[a,b,1], Weiwei Fan[b], Katrina G. Waymire[b,c], Alfredo A. Sadun[d], Valerio Carelli[d,e,f], Fred N. Ross-Cisneros[d], Peter Baciu[g], Eric Sung[g], Meagan J. McManus[a], Billy X. Pan[d], Daniel W. Gil[g], Grant R. MacGregor[b,c], and Douglas C. Wallace[a,b,h,2]

[a]Center for Mitochondrial and Epigenomic Medicine, Children's Hospital of Philadelphia, Philadelphia, PA 19104; [b]Center for Molecular and Mitochondrial Medicine and Genetics and Department of Biological Chemistry, University of California, Irvine, CA 92697; [c]Department of Developmental and Cell Biology, University of California, Irvine, CA 92697-2300; [d]Departments of Ophthalmology and Neurological Surgery, Doheny Eye Institute, University of Southern California (USC) Keck School of Medicine, Los Angeles, CA 90089-0228; [e]Istituto delle Scienze Neurologiche di Bologna, Istituiti di Ricovero e Cura a Carattere Scientifico (IRCCS), Bologna, Italy; [f]Department of Neurological Sciences, University of Bologna School of Medicine, Bologna, Italy; [g]Department of Biological Sciences, Allergan, Inc., Irvine, CA 92612; and [h]Department of Pathology and Laboratory Medicine, University of Pennsylvania, Philadelphia, PA 19104

Contributed by Douglas C. Wallace, October 7, 2012 (sent for review September 10, 2012)

An animal model of Leber hereditary optic neuropathy (LHON) was produced by introducing the human optic atrophy mtDNA *ND6* P25L mutation into the mouse. Mice with this mutation exhibited reduction in retinal function by elecroretinogram (ERG), age-related decline in central smaller caliber optic nerve fibers with sparing of larger peripheral fibers, neuronal accumulation of abnormal mitochondria, axonal swelling, and demyelination. Mitochondrial analysis revealed partial complex I and respiration defects and increased reactive oxygen species (ROS) production, whereas synaptosome analysis revealed decreased complex I activity and increased ROS but no diminution of ATP production. Thus, LHON pathophysiology may result from oxidative stress.

neurodegenerative disease | maternal inheritance | oxidative phosphorylation | ophthalmology

Leber hereditary optic neuropathy (LHON), the first inherited mitochondrial (mt)DNA disease reported (1), is thought to be one of the most prevalent diseases caused by mtDNA missense mutations, having an estimated frequency of 15 in 100,000 (2). Most European LHON mutations occur in the mtDNA oxidative phosphorylation (OXPHOS) complex I (NADH:ubiquinone oxidoreductase or NADH dehydrogenase) genes, the three most common being the *ND4* gene mutation at nucleotide G11778A causing an arginine 340 to histidine (R340H) substitution (1), the *ND1* G3460A (A52T) mutation (3), and the *ND6* T14484C (M64V) mutation (4). Milder LHON mutations are generally homoplasmic (pure mutant). In contrast, more severe mtDNA complex I *ND* gene mutations can cause basal ganglia degeneration presenting as dystonia or Leigh syndrome when homoplasmic but optic atrophy when heteroplasmic (mixed mutant and normal mtDNAs). Two examples of such mutations are *ND6* G14459A (A72V) (5) and *ND6* G14600A (P25L) (6).

LHON generally presents in the second or third decade of life as acute or subacute onset of central vision loss, first in one eye and then in the other. The percentage of optic atrophy in patients varies markedly among pedigrees. Male patients are two to five times more likely to develop blindness than female patients (2), and maternal relatives who have not progressed to subacute optic atrophy can still show signs of visual impairment (7, 8).

In LHON, optic atrophy is associated with preferential loss of the central small-caliber optic nerve fibers of the papillomacular bundle, resulting in central scotoma but with sparing of the larger-caliber peripheral fibers and retention of peripheral vision. The loss of the optic nerve fibers is attributed to the death of retinal ganglion cells (RGC) as a result of the high energy demand placed on the unmyelinated portion of the optic nerve fibers anterior to the lamina cribosa, an area associated with high mitochondrial density (2).

Complex I is the largest and most intricate of the mitochondrial OXPHOS complexes. It is comprised of 45 subunits, 7 (ND1, -2, -3, -4, -4L, -5, and -6) of which are coded by the mtDNA (9). Complex I transfers electrons from NADH to ubiquinone, and the energy released from this redox reaction is coupled to pumping protons across the mitochondrial inner membrane to create an electrochemical gradient, which can be used by the H^+-translocating ATP synthase (complex V or ATP synthase) to condense ADP plus P_i into ATP. Complex I is a major site for reactive oxygen species (ROS) produced in the mitochondrial matrix (10).

The biochemical basis of LHON has been investigated by transferring mutant mtDNAs into cultured cells by fusion of patient platelets or cytoplasts to established human cells lacking mtDNA (ρ^o cells). Subsequent analysis of these cybrids (11) have revealed partial complex I and site I respiration defects, reduced ATP production, increased mitochondrial ROS production, sensitization of the mitochondrial permeability transition pore (mtPTP) with predilection to apoptosis, and oxidative stress–induced inhibition of the excitatory glutamate transporter 1 (12–23).

Although these studies have elucidated many biochemical aspects of LHON, they have not revealed why only particular complex I gene mutations present with optic atrophy, why RGCs and the optic nerve are preferentially affected even though the mtDNA mutation is present throughout the body, and what is the relationship between the severity of the mutation and the varying consequences for the optic nerve and the basal ganglia.

To address these and other questions, a mouse model of LHON is required that harbors the equivalent mtDNA mutation, as found in optic atrophy patients. Therefore, we needed to isolate such a mouse mtDNA mutation, introduce the mutant mtDNA into the mouse female germ line, and demonstrate that the mouse acquired an ophthalmological phenotype. The biochemical consequences of the mutation in the nervous system could then be investigated.

Because the mouse has a much shorter life span than humans, we reasoned that a LHON mutation causing optic atrophy in the mouse within 2 y would need to be equivalent to one of the more severe mutations in humans that cause optic atrophy in 20 y. Such human mutations would cause optic atrophy when heteroplasmic but dystonia or Leigh syndrome when homoplasmic.

Author contributions: C.S.L., M.S.S., A.A.S., M.J.M., D.W.G., G.R.M., and D.C.W. designed research; C.S.L., M.S.S., W.F., K.G.W., V.C., F.N.R.-C., P.B., E.S., M.J.M., B.X.P., and G.R.M. performed research; W.F., K.G.W., and G.R.M. contributed new reagents/analytic tools; C.S.L., M.S.S., W.F., A.A.S., V.C., F.N.R.-C., P.B., E.S., M.J.M., B.X.P., and G.R.M. analyzed data; and C.S.L., M.S.S., and D.C.W. wrote the paper.

The authors declare no conflict of interest.

Freely available online through the PNAS open access option.

[1]C.S.L. and M.S.S. contributed equally to this work.

[2]To whom correspondence should be addressed. E-mail: wallaced1@email.chop.edu.

This article contains supporting information online at www.pnas.org/lookup/suppl/doi:10.1073/pnas.1217113109/-/DCSupplemental.

We now report the production of a mouse that harbors the equivalent of the human *ND6* G14600A P25L mutation. Despite the inherent anatomical and functional differences between the human and mouse eye, mice with this mutation develop optic atrophy that closely models LHON pathology. As expected, both nervous and nonnervous tissue of the *ND6* P25L mouse showed reduced complex I activity and increased ROS production during NADH-driven electron transport through complex I. However, the *ND6* P25L synaptosomes produced increased ROS but were able to maintain ATP levels even under increased energetic demand. This suggests that oxidative stress rather than energy deficiency may be the important factor in LHON pathophysiology.

Results

Generation of Mice Harboring a Human Optic Atrophy mtDNA Mutation. We used a multistep approach to isolate a mouse cell line that harbored a human-equivalent mtDNA mutation. First, LMTK$^-$ cells were mutagenized with psoralen and UV light. Mutant mtDNA species were enriched by ethidium bromide depletion–reamplification and cloning. Next, clones were screened for partial respiratory defects by glucose–galactose selection (24). Finally, mtDNAs were sequenced from multiple clones to identify one that harbored a mutation associated with human optic atrophy. Clone LT13 was homoplasmic for a *ND6* gene mutation at nucleotide G13997A, which causes a *ND6* P25L amino acid substitution, the same amino acid substitution as reported in a *ND6* G14600A (P25L) optic atrophy and Leigh syndrome family (6).

Mitochondrial OXPHOS analysis of LT13 versus LMTK$^-$ cells revealed that the *ND6* P25L mutation reduced complex I–specific activity by 23% (Fig. S1*A*) without altering the physical integrity of complex I (Fig. S1*B*). Although the specific activities of complex II plus III and citrate synthase (Fig. S1 *C* and *D*) were not altered, the complex IV activity was increased by 31%, presumably as a compensatory reaction to the complex I defect (25) (Fig. S1*E*). The complex I defect was associated with a 24% reduction in mitochondrial respiration using NADH-linked substrates malate and pyruvate, whereas succinate-driven respiration was normal (Fig. S1*F*). This was paralleled by a 65% reduction in ATP-synthesis rate (Fig. S1*G*) and a 48% increase in mitochondrial ROS production (Fig. S1*H*). Hence, the *ND6* nucleotide G13997A P25L mutation met the criteria for a mouse mutant equivalent to that of a human LHON mutation.

The LT13 cell line was enucleated, and the mtDNA-containing cytoplast was fused to 129SvEv (129S6) female mouse embryonic stem cell (fmESC) line (CC9.3.1), the resident 129S6 mDNAs having been removed before fusion by transient treatment with rhodamine-6G (11, 26). The resulting fmESC containing the homoplasmic *ND6* nucleotide G13997A P25L mutation were injected into blastocysts, chimeric females were identified (27), and the maternal transmission of homoplasmic *ND6* G13997A mtDNA mutant was confirmed by mtDNA sequencing. Females harboring the G13997A mutation were backcrossed with C57BL/6J males for over 10 generations, resulting in viable, fertile, mtDNA *ND6* G13997A P25L mutant mice.

Reduced Retinal Response in *ND6* P25L Mice. The *ND6* P25L mice were first examined for ocular function by electroretinogram (Table 1). The 14-mo-old mice showed a significant deficit in nearly all parameters examined. The scotopic B wave of dark-adapted *ND6* P25L eyes was reduced in amplitude by 25.5% and 33.1% with 0.01 and 1 cd·s/m^2 (maximum) stimulations. The scotopic A-wave of *ND6* P25L mutant eyes displayed a 23% reduction. The scotopic oscillatory potentials (OPs), a high-frequency response derived from multiple retinal cell types, showed a 20.7% and 21.7% reduction with 0.01 and 1 cd·s/m^2 stimulations. Photopic B-wave ERG amplitude, measuring cone functions, was decreased 17.7%. There was also a trend toward increased latencies to the A and B waves (Table S1). Despite the functional deficit observed in the ERGs, the *ND6* P25L mice did not exhibit reduced visual responses as assessed by optokinetic analysis (Fig. S2).

RGC Axonal Swelling and Preferential Loss of Smallest Fibers in the *ND6* P25L Mice. Electron microscopic analysis of RGC axons revealed that the *ND6* P25L eyes exhibited axonal swelling in their optic nerves (Fig. 1 *A* and *B* and Fig. S3 *A* and *B*). The average axonal diameter was 0.67 ± 0.01 μm in wild-type and 0.80 ± 0.04 μm ($P < 0.0001$) in *ND6* P25L mutant 14-mo-old mice and 0.73 ± 0.01 μm in wild-type and 0.85 ± 0.05 μm in *ND6* P25L mutant ($P < 0.0001$) mice at 24 mo (Fig. 1*C*). Fourteen-month-old ND6 mutant mice had an increased number of large fibers but fewer small axonal fibers (≤0.5 μm). The change in axonal diameters was more pronounced in 24-mo-old *ND6* P25L mice (Fig. 1*D*). Hence, *ND6* P25L mice have fewer small and medium axons (≤0.8 μm) and more swollen axonal fibers with diameters larger than 1 μm. This was most severe in the area of the smallest fibers, which are found in the central and temporal regions of the mouse optic nerve, which corresponds to the human temporal region most affected in LHON (Fig. S4).

Quantification of the number of axons in the optic nerves revealed no difference in the total counts at 14 mo but a 30% reduction at 24 mo ($P < 0.0001$) (Fig. 1*E*). Thus, the observed shift toward larger axons is initially (14 mo) attributable to swelling of medium axons and, later (24 mo), the loss of small axons.

Abnormal Mitochondrial Morphology and Proliferation in RGC Axons of *ND6* P25L Mice. Mitochondria in the optic tracts of the *ND6* P25L mutants were abnormal and increased in number, consistent with the compensatory mitochondrial proliferation observed in LHON patients (Fig. 2*A* and Fig. S5*A*). The optic tract axons of 14-mo-old *ND6* P25L mice had a 58% increase in mitochondria ($P = 0.0036$) (Fig. 2*B*), whereas those at 24 mo had a 94% increase ($P = 0.064$) (Fig. 2*C*). The *ND6* P25L mitochondria often appeared to be hollowed and possessed irregular cristae (Fig. 2*D* and Fig. S5*B*), with 31.5% more of the *ND6* P25L mitochondria being abnormal at 14 mo ($P = 0.23$; Fig. 2*E*) and 56% more at 24 mo ($P = 0.03$; Fig. 2*F*). Axons filled with abnormal mitochondria often demonstrated marked thinning of the myelin sheath (Fig. 2*A* and Fig. S5*A*).

Table 1. ERG responses

	Scotopic B wave			Scotopic oscillatory potential		
Mouse strain	0.01 cd·s/m^2	1 cd·s/m^2	Scotopic A wave (1 cd·s/m^2)	0.01 cd·s/m^2	1 cd·s/m^2	Photopic B wave
Control	483.8 ± 22.68*	743.0 ± 25.38†	345.7 ± 12.81†	24.33 ± 1.087*	53.87 ± 2.091†	86.89 ± 5.406‡
ND6 (P25L)	351.9 ± 23.00*	553.3 ± 39.68*	266.2 ± 18.61*	19.30 ± 1.487*	42.17 ± 3.620*	71.50 ± 6.187‡
	($P = 0.0003$)	($P = 0.0004$)	($P = 0.0016$)	($P = 0.0104$)	($P = 0.0101$)	($P = 0.0757$)

All values are amplitudes (microvolts) ± SEM .
*$n = 16$.
$^\dagger n = 15$.
$^\ddagger n = 11$.

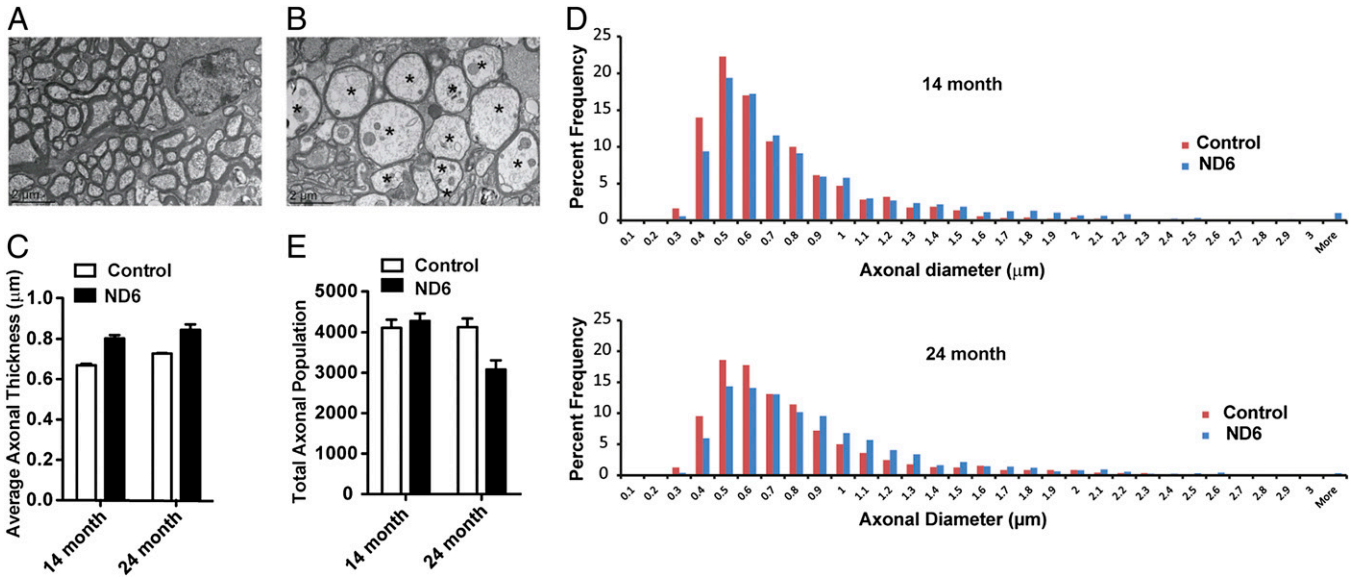

Fig. 1. Ultrastructural analysis of RGC axons showing swelling and loss in ND6 mutant mice. (*A* and *B*) Fourteen-month-old wild-type (*A*) and 14-mo-old ND6 mutant (*B*) mouse retrobulbar optic nerves at 2,000× magnification. Several swollen axons with thin myelin (asterisks) can be seen adjacent to normal caliber axons (*Lower Left*) from a 14-mo-old ND6 mutant mouse. EM images of 24-mo-old axons can be found in Fig. S3. (*C*) Average axonal diameter in the 14- and 24-mo-old control and ND6 mutant mice ($n = 4$). (*D*) Histograms of percentage distribution of optic nerve axon diameters in both 14- and 24-mo-old wild-type and ND6 mutant mice (bin size, 0.1 μm). A total of 1,600 individual axons were sampled separately for 14- and 24-mo-old mutant groups. A total of 1,600 and 1,200 axons were counted for 12- and 24-mo-old wild type. The distribution of axonal diameters in the 14-mo age group showed a shift in the ND6 mutant subset to larger diameter axons, whereas those smaller than 0.5 μm in diameter were reduced in number. This trend was augmented in 24-mo age group. (*E*) Total axonal population determined from cross sections of optic nerve.

Altered Liver Mitochondria Complex I Activity in *ND6* P25L Mice. The complex I activity of the *ND6* P25L mice, assayed in liver mitochondria, revealed that the rotenone-sensitive NADH:ubiquinone oxidoreductase activity was decreased by 29% ($P = 0.0119$; Fig. 3*A*), equivalent to the reduction seen in the LT13 cell line (Fig. S1*A*). The decrease in activity was not attributable to a lower abundance of complex I, because the NADH:ferricyanide oxidoreductase was unaltered in the ND6 mutant mice (Fig. 3*B*). The

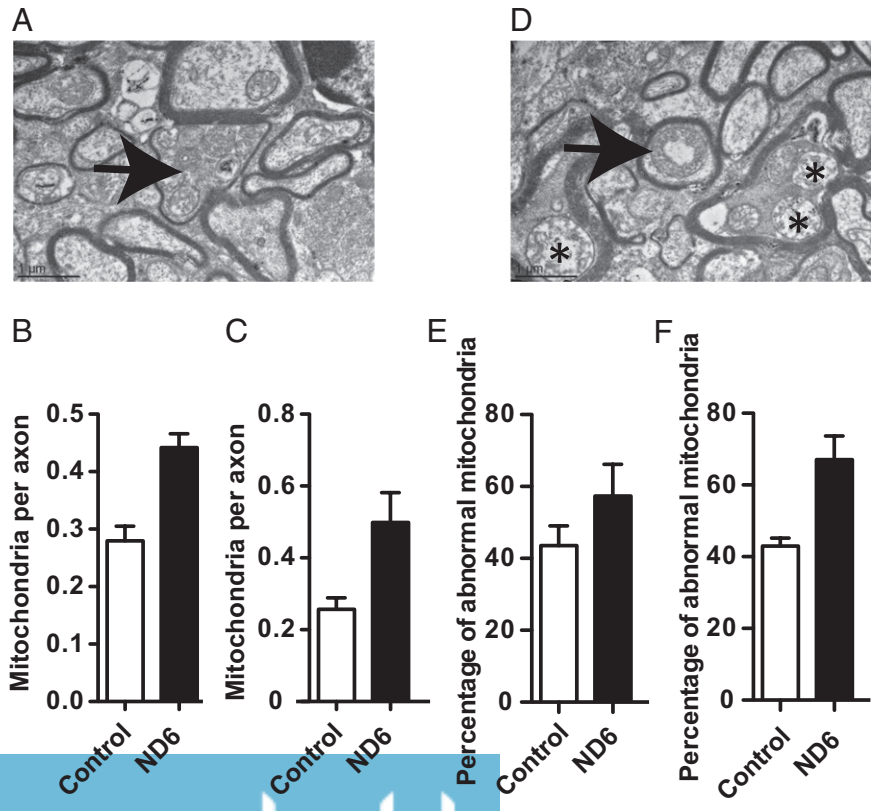

Fig. 2. Ultrastructural analysis of optic nerve showing mitochondrial abnormalities in ND6 mutant mice. Quantification of mitochondria by transmission electron microscopy (EM) (4,000×). (*A*) The arrow indicates an axon of 14-mo-old ND6 mutant mouse characterized by mitochondrial proliferation and marked thinning of the myelin sheath. (*B* and *C*) Number of mitochondria per axon in optic nerves from 14-mo-old mice [control ($n = 4$): 267 mitochondria in 954 axons; mutant ($n = 4$): 427 mitochondria in 964 axons] (*B*) and 24-mo-old mice [control ($n = 3$): 188 mitochondria in 723 axons; mutant ($n = 4$): 384 mitochondria in 801 axons] (*C*). See Fig. S5*A* for mitochondrial proliferation at 24 mo. (*D*) Abnormal mitochondrial morphology as seen with central vacuolization *(arrow)* and disrupted cristae (asterisks) in 14-mo-old ND6 mutant. See Fig. S5*B* for mitochondrial abnormalities at 24 mo. (*E* and *F*) Percentage of abnormal mitochondria in the optic nerves of 14-mo-old mice (*E*) and in the optic nerves of 24-mo-old mice (*F*).

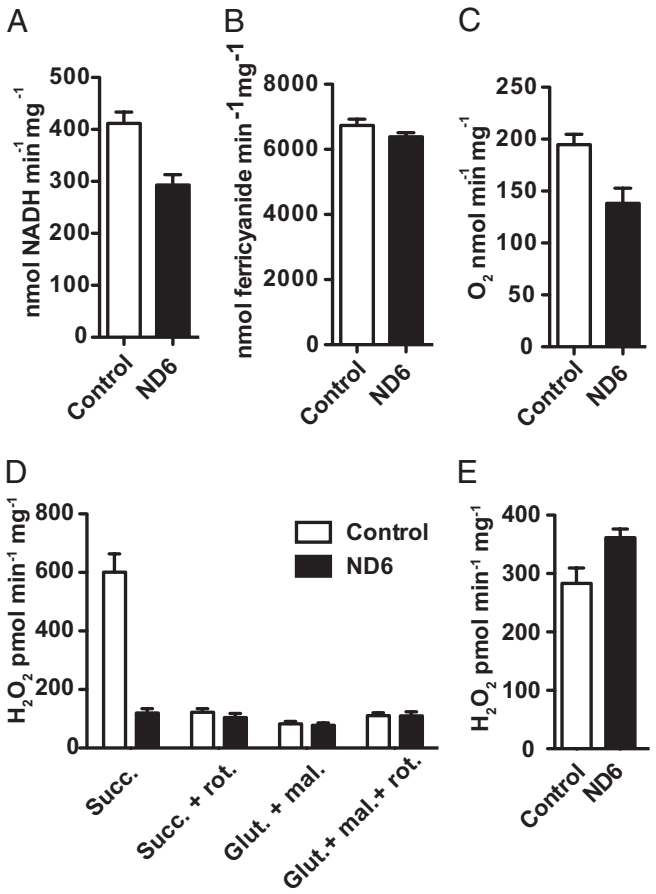

Fig. 3. Complex I–related biochemistry in liver mitochondria isolated from ND6 mutant liver. (*A*) Rotenone-sensitive NADH:coenzyme Q_1 oxidoreductase activity of liver mitochondria isolated from ND6 mutant mice and control animals ($n = 5$). (*B*) NADH:ferricyanide oxidoreductase activity of liver mitochondria ($n = 5$). (*C*) Maximal respiration rate of isolated liver mitochondria measured by polarography using glutamate and malate as substrates in the presence of excess ADP (2 mM) ($n = 9$). (*D*) Hydrogen peroxide production by isolated liver mitochondria using Amplex red to detect mitochondrial hydrogen peroxide efflux ($n = 9$). (*E*) Hydrogen peroxide production determined in SMPs prepared from liver mitochondria ($n = 2$). N refers to independent preparations of mitochondria or SMPs, and the assays were performed at least in triplicate for each preparation.

ND6 mutation also caused a 25% decrease in mitochondrial oxygen consumption ($P = 0.0152$; Fig. 3*C*), also seen in the LT13 cell line (Fig. S1*F*).

Increased Forward Electron Flow but Lack of Reverse Electron Flow ROS Production in *ND6* P25L Liver Mitochondria. Analysis of mitochondrial H_2O_2 production in *ND6* P25L mutant liver mitochondria revealed little difference in ROS production using site 1 substrates (glutamate and malate) (Fig. 3*D*). However, when complex I H_2O_2 production was measured during reverse electron transfer (RET) driven by succinate in the presence of oligomycin, the *ND6* P25L mutation had an almost complete absence of ROS production (Fig. 3*D*).

Because the measurable rate of H_2O_2 production during forward electron transfer was lower than seen in the LT13 cells (Fig. S1*H*), we tested submitochondrial particles (SMPs), which lack much of the H_2O_2-detoxification systems. The *ND6* P25L mouse SMPs had a significant increase in H_2O_2 production during forward electron transfer (Fig. 3*E*), comparable to that seen in LT13 cells.

Reduced Complex I Activity and Increased Forward but Not Reverse ROS Production in *ND6* P25L Synaptosomes. To evaluate the consequences of the *ND6* P25L mutation in neuronal cells, mitochondrial function was examined in isolated synaptosomes, plasma membrane–bound synaptic boutons that encompass mitochondria and cytoplasmic biochemical machinery of the neuron. *ND6* P25L mutant synaptosomes had reduced oxygen consumption under all conditions examined (Fig. 4*A*). However, this reduction was greatest under low-turnover conditions (basal or in the presence of oligomycin), whereas the deficit decreased as the mitochondrial membrane potential was reduced and respiration rate increased due to uncoupling with carbonyl cyanide-4-(trifluoromethoxy)phenylhydrazone (FCCP) or by activating the plasma membrane sodium ion channel with veratridine, thus increasing ATP consumption by the Na^+-K^+ ATPase (Fig. 4*A*). In contrast to cultured cell mitochondria in which ATP production was reduced (Fig. S1*G*), in situ ATP levels in the synaptosomes were maintained under various energetically demanding conditions, including incubation with 4-aminopyridine, a potassium ion channel inhibitor; a high concentration of KCl that depolarizes synaptosome; and veratridine (Fig. 4*B*). The *ND6* P25L synaptosomes did display a slight but significantly greater decrease in ATP levels than control mice when partially inhibited by rotenone (9.7% less than controls; $P = 0.0173$) (Fig. 4*C*), a phenomenon previously reported for cybrid cell lines harboring LHON mtDNA mutations (19, 28–30).

Analysis of brain mitochondrial H_2O_2 production revealed that *ND6* P25L mitochondria had elevated ROS production during forward complex I electron transport from glutamate and malate but marked suppression of ROS production during RET from succinate in the presence of oligomycin (Fig. 4*D*). Rotenone increased the rate of H_2O_2 production during forward electron transfer in both wild-type (2.3-fold increase) and *ND6* P25L (2.7-fold increase) synaptosomes. Therefore, the *ND6* P25L brain mitochondria have an increased rate of H_2O_2 generation even if electron transfer to ubiquinone is fully inhibited by rotenone (*ND6* P25L: 1,339 pmol·min^{-1}·mg^{-1}; wild-type: 999 pmol·min^{-1}·mg^{-1}; Fig. 4*D*). During RET conditions, with succinate plus oligomycin, rotenone decreased the rate of generation of H_2O_2 in wild-type animals by 79% and in *ND6* P25L mice by 59%. In these conditions the rate of H_2O_2 generation is equivalent for wild-type (1,190 pmol·min^{-1}·mg^{-1}) and *ND6* P25L (1,138 pmol·min^{-1}·mg^{-1}) mice (Fig. 4*D*).

Synaptosomes respiring on glucose also had increased forward electron transfer H_2O_2 production (37% increase; $P = 0.015$), and this increase was also preserved in the presence of rotenone (37% increase; $P = 0.0462$) (Fig. 4*E*). These biochemical differences are kinetic in nature because complex I subunit levels were not decreased (Fig. S6).

To determine whether the increased ROS production has cellular consequences, 3-nitrotyrosine and glial fibrillary acid protein (GFAP) levels were measured. The 3-nitrotyrosine level was increased more than twofold (236%; $P < 0.0001$), and GFAP was increased by 65.5% ($P = 0.0059$) (Fig. 4 *F* and *G*).

Discussion

We isolated a mtDNA mutation (*ND6* nucleotide G13997A P25L) in mouse C3H L cells (31), resulting in the same amino acid substitution (*ND6* P25L) found in a patient with optic atrophy and cerebellar ataxia (6). This mtDNA mutant resulted in a partial complex I defect and increased ROS production and when introduced into the mouse optic atrophy. Surprisingly, this same mutation arose independently in C57BL Lewis lung tumor cells (32) on a different mtDNA background (Table S2) and, when introduced into mice, caused altered glucose metabolism and late-onset lymphoma (33). The isolation of the same mutation twice suggests it may be advantageous in cultured cells (34).

Mice harboring our L cell–derived *ND6* G13997A P25L mtDNA mutation exhibited all of the features of human LHON

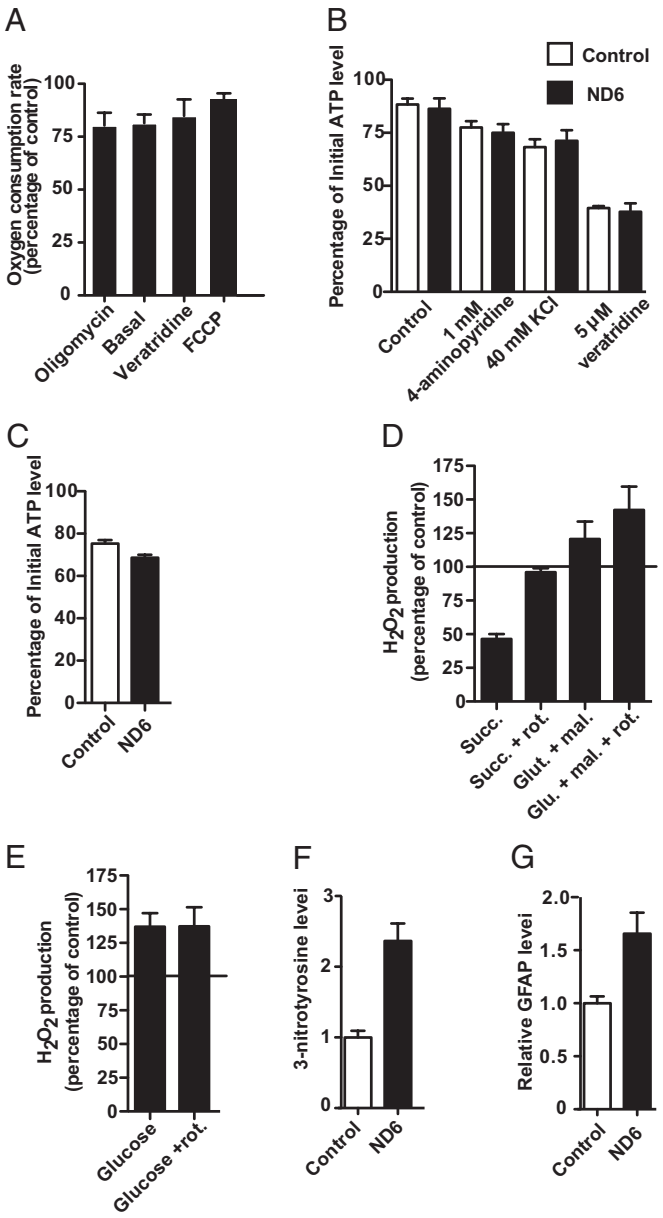

Fig. 4. Bioenergetic and oxidative stress consequences of the ND6 mutation in neuronal tissue. (*A*) Oxygen consumption rate (OCR) of synaptosomes in the presence of 1 μg·mL^{-1} oligomycin, 5 μM veratridine, and 4 μM FCCP ($n = 6$). The reported results are the OCR of synaptosomes from the ND6 mutant mice expressed as a percentage of the rate of synaptosomes isolated from control mice. (*B*) Ability of synaptosomes from control and ND6 mutant to maintain ATP levels under energetically demanding conditions. The ATP levels of synaptosomes were determined before and after 15 min of incubation without (control) or with plasma membrane–depolarizing agents, and the results are expressed as the percentages of the initial ATP level ($n = 7$). In *ND6* P25L mice, the initial ATP levels were 126,535 ± 14,871 relative light units (RLU)/25 μg of synaptosomes, and in B6 control mice, the initial ATP levels were 126,663 ± 10,264 RLU/25 μg. (*C*) ability of synaptosomes to maintain ATP levels in the presence of 100 nM rotenone ($n = 3$). (*D*) Rate of hydrogen peroxide production by nonsynaptosomal brain mitochondria measured using the Amplex red system ($n = 5$). The rate is expressed as the percentage difference between mitochondria isolated from the *ND6* mutant and control mice at the same time. (*E*) Rate of hydrogen peroxide generation from synaptosomes in the presence and absence of rotenone (4 μM) using glucose as a substrate ($n = 7$). The rate is expressed as the percentage. (*F* and *G*) Immunoblotting of 3-nitrotyrosine (*F*) and GFAP (*G*) levels in whole-brain lysates ($n = 5$). N refers to independent preparations of mitochondria, synaptosomes, or whole-cell lysates. Assays were performed at least in triplicate for each preparation.

possible given the anatomical differences between the human and mouse eye. The *ND6* P25L mice showed reductions in ERG amplitudes and aggregate retinal cell oscillatory potentials and increased response latencies. Partial retinal deficiencies including reduced ERG cone responses have been seen in LHON asymptomatic carriers and LHON patients (35, 36).

The *ND6* P25L mice exhibited an age-related loss of small-caliber optic nerve fibers while preserving the large-caliber peripheral optic nerve fibers, with the total axonal counts of the mutant optic nerves being significantly reduced by 24 mo, and yet the mice remained responsive to light, possibly suggesting retention of peripheral vision. The mutant neurons gave rise to swollen, demyelinated fibers that harbored increased numbers of highly abnormal mitochondria. Small caliber axonal loss and fiber swelling in association with abnormal mitochondria is a hallmark for LHON pathology (28, 37, 38).

This optic nerve pathology was associated with a systemic decrease in mitochondrial complex I–specific activity and respiration and an increase in complex I ROS production during forward electron flow, confirmed in both liver and brain mitochondria. However, the *ND6* P25L mutation was also associated with an almost complete absence of complex I RET ROS production.

Two sites in complex I have been proposed to produce superoxide anion: the coenzyme Q_{10} (CoQ)-binding site (10, 39) and the flavin mononucleotide (FMN) (40). Because the *ND6* P25L complex I mutant does not generate ROS by RET but does during forward electron transport, even in the presence of rotenone, the primary site for ROS production must be upstream of the rotenone- and ubiquinone-binding sites (40), most likely at FMN or possibly in some unknown mutant-specific site.

In synaptosomes the *ND6* P25L mutation does not lead to a proximal energetic defect, because the mutant mice can maintain ATP homeostasis even under energetically demanding conditions. However, the mutation does cause an increase in ROS production and oxidative damage. If the biochemical alterations associated with the *ND6* G14600A/G13997A (P25L) human and mouse mutations are characteristic of the LHON *ND6* G14459A (A72V), *ND4* G11778A (R340H), *ND1* G3460A (A52T), and *ND6* T14484C (M64V) mutations, our synaptosome results suggest that the pathophysiology of LHON is less about ATP deficiency and more about chronic oxidative damage, consistent with the sensitization of mtPTP in LHON mtDNA cybrids (41, 42).

In conclusion, we have generated a mouse model of LHON by introducing into the mouse a known mtDNA optic atrophy mutation (*ND6* P25L). The *ND6* P25L mutation causes a systemic complex I defect and associated increased ROS production but, in synaptosomes (and presumably in the RGCs and optic nerve), causes chronically increased ROS production even when electron transfer to ubiquinone is inhibited without significantly reducing neuronal ATP production. Therefore, chronic oxidative stress rather that energy deficiency appears to be the clinically relevant factor in LHON. If so, then mitochondria-targeted catalytic antioxidant therapeutics (43–45) might be an effective way to prevent the onset of central scotoma in carriers of LHON mtDNA mutations.

Materials and Methods

All experimental procedures involving mice were conducted in accordance to approved Institutional Animal Care and Use Committee (IACUC) protocols of the Children's Hospital of Philadelphia.

Generation of a Transgenic Mouse Harboring *ND6* P25L mtDNA Mutation. The fibroblast cell line, LMTK$^-$, was treated with trimethyl psoralen (30–3 μg·mL^{-1}) for 2 d (24). The dishes were exposed to UV irradiation and ethidium bromide treatment for 10 d to deplete mtDNA. Fibroblasts with mutant mtDNA species were identified through inhibition of growth on galactose medium, cloning, and sequencing (24).

ND6 P25L mutant fibroblasts were enucleated by either actinomycin D (0.5 μg·mL^{-1}) (46) or by cytochalasin B (20 μg·mL^{-1}) treatment, together with ultracentrifugation in discontinuous Ficoll gradients (47); 129S6 mouse female

embryonic stem (ES) cells, CC9.3.1, were treated with rhodamine-6G (0.75 $\mu g \cdot mL^{-1}$) to deplete the resident mtDNAs; and the *ND6* P25L mutant cytoplasts were fused with ES cells using polyethylene glycol. ES fusions were selected in hypoxanthine–aminopterin–thymidine (HAT) media (26, 27). Homoplasmic mtDNA *ND6* G13997A P25L CC9.3.1 transmitochondrial cybrid clones were injected into C57BL/6NHsd blastocysts, which were implanted into pseudopregnant females (48). Chimeric female offspring were mated to obtain germ-line transmission of the *ND6* mutation. Females with the mutation were backcrossed with Jackson Laboratory C57BL/6J (stock no. 000664) males for at least 10 generations.

Anatomical, Functional and Physiological Analysis. Methods of electroretinography, biochemistry, histology, immunoblotting, and statistical analysis are detailed in *SI Materials and Methods*.

ACKNOWLEDGMENTS. This work was supported by National Institutes of Health (NIH) Grants NS21328, NS41850, AG24373, and DK73691 and Simons Foundation Grant 205844 (to D.C.W.). This study was also supported by the International Foundation for Optic Nerve Diseases (IFOND), Struggling Within Leber's, the Poincenot Family for LHON Research, the Eierman Foundation, Research to Prevent Blindness, and NIH Grant EY03040 (to A.A.S., F.N.R.-C., and B.X.P.).

1. Wallace DC, et al. (1988) Mitochondrial DNA mutation associated with Leber's hereditary optic neuropathy. *Science* 242(4884):1427–1430.
2. Sadun AA, La Morgia C, Carelli V (2011) Leber's hereditary optic neuropathy. *Curr Treat Options Neurol* 13(1):109–117.
3. Huoponen K, Vilkki J, Aula P, Nikoskelainen EK, Savontaus ML (1991) A new mtDNA mutation associated with Leber hereditary optic neuroretinopathy. *Am J Hum Genet* 48(6):1147–1153.
4. Johns DR, Neufeld MJ, Park RD (1992) An ND-6 mitochondrial DNA mutation associated with Leber hereditary optic neuropathy. *Biochem Biophys Res Commun* 187(3): 1551–1557.
5. Jun AS, Brown MD, Wallace DC (1994) A mitochondrial DNA mutation at np 14459 of the ND6 gene associated with maternally inherited Leber's hereditary optic neuropathy and dystonia. *Proc Natl Acad Sci USA* 91(13):6206–6210.
6. Malfatti E, et al. (2007) Novel mutations of ND genes in complex I deficiency associated with mitochondrial encephalopathy. *Brain* 130(Pt 7):1894–1904.
7. Savini G, et al. (2005) Retinal nerve fiber layer evaluation by optical coherence tomography in unaffected carriers with Leber's hereditary optic neuropathy mutations. *Ophthalmology* 112(1):127–131.
8. Ventura DF, et al. (2007) Male prevalence of acquired color vision defects in asymptomatic carriers of Leber's hereditary optic neuropathy. *Invest Ophthalmol Vis Sci* 48 (5):2362–2370.
9. Hirst J (2010) Towards the molecular mechanism of respiratory complex I. *Biochem J* 425(2):327–339.
10. Murphy MP (2009) How mitochondria produce reactive oxygen species. *Biochem J* 417 (1):1–13.
11. Trounce IA, Kim YL, Jun AS, Wallace DC (1996) Assessment of mitochondrial oxidative phosphorylation in patient muscle biopsies, lymphoblasts, and transmitochondrial cell lines. *Methods Enzymol* 264:484–509.
12. Jun AS, Trounce IA, Brown MD, Shoffner JM, Wallace DC (1996) Use of transmitochondrial cybrids to assign a complex I defect to the mitochondrial DNA-encoded NADH dehydrogenase subunit 6 gene mutation at nucleotide pair 14459 that causes Leber hereditary optic neuropathy and dystonia. *Mol Cell Biol* 16(3):771–777.
13. Jun AS, Trounce IA, Brown MD, Shoffner JM, Wallace DC (1996) Use of transmitochondrial cybrids to assign a complex I defect to the mitochondrial DNA-encoded NADH dehydrogenase subunit 6 gene mutation at nucleotide pair 14459 that causes Leber hereditary optic neuropathy and dystonia. *Mole Cell Biol* 16(3):771–777.
14. Brown MD, Allen JC, Van Stavern GP, Newman NJ, Wallace DC (2001) Clinical, genetic, and biochemical characterization of a Leber hereditary optic neuropathy family containing both the 11778 and 14484 primary mutations. *Am J Med Genet* 104(4): 331–338.
15. Brown MD, Trounce IA, Jun AS, Allen JC, Wallace DC (2000) Functional analysis of lymphoblast and cybrid mitochondria containing the 3460, 11778, or 14484 Leber's hereditary optic neuropathy mitochondrial DNA mutation. *J Biol Chem* 275(51): 39831–39836.
16. Carelli V, et al. (1999) Biochemical features of mtDNA 14484 (ND6/M64V) point mutation associated with Leber's hereditary optic neuropathy. *Ann Neurol* 45(3): 320–328.
17. Carelli V, et al. (1997) Leber's hereditary optic neuropathy: Biochemical effect of 11778/ND4 and 3460/ND1 mutations and correlation with the mitochondrial genotype. *Neurology* 48(6):1623–1632.
18. Baracca A, et al. (2005) Severe impairment of complex I-driven adenosine triphosphate synthesis in leber hereditary optic neuropathy cybrids. *Arch Neurol* 62(5): 730–736.
19. Beretta S, et al. (2006) Partial mitochondrial complex I inhibition induces oxidative damage and perturbs glutamate transport in primary retinal cultures. Relevance to Leber Hereditary Optic Neuropathy (LHON). *Neurobiol Dis* 24(2):308–317.
20. Floreani M, et al. (2005) Antioxidant defences in cybrids harboring mtDNA mutations associated with Leber's hereditary optic neuropathy. *FEBS J* 272(5):1124–1135.
21. Ghelli A, et al. (2008) Protection against oxidant-induced apoptosis by exogenous glutathione in Leber hereditary optic neuropathy cybrids. *Invest Ophthalmol Vis Sci* 49(2):671–676.
22. Sala G, et al. (2008) Antioxidants partially restore glutamate transport defect in leber hereditary optic neuropathy cybrids. *J Neurosci Res* 86(15):3331–3337.
23. Giordano C, et al. (2011) Oestrogens ameliorate mitochondrial dysfunction in Leber's hereditary optic neuropathy. *Brain* 134(Pt 1):220–234.
24. Acín-Pérez R, et al. (2004) Respiratory complex III is required to maintain complex I in mammalian mitochondria. *Mol Cell* 13(6):805–815.
25. Fan W, et al. (2008) A mouse model of mitochondrial disease reveals germline selection against severe mtDNA mutations. *Science* 319(5865):958–962.
26. Sligh JE, et al. (2000) Maternal germ-line transmission of mutant mtDNAs from embryonic stem cell-derived chimeric mice. *Proc Natl Acad Sci USA* 97(26):14461–14466.
27. MacGregor GR, Fan WW, Waymire KG, Wallace DC (2006) Generating animal models of human mitochondrial genetic disease using mouse ES cells. *Embryonic Stem Cells, Practical Approach Series*, eds Notarianni E, Evans MJ (Oxford University Press, New York, NY), pp 72–104.
28. Marella M, Seo BB, Thomas BB, Matsuno-Yagi A, Yagi T (2010) Successful amelioration of mitochondrial optic neuropathy using the yeast NDI1 gene in a rat animal model. *PLoS ONE* 5(7):e11472.
29. Cock HR, Cooper JM, Schapira AH (1999) Functional consequences of the 3460-bp mitochondrial DNA mutation associated with Leber's hereditary optic neuropathy. *J Neurol Sci* 165(1):10–17.
30. Silva JM, Wong A, Carelli V, Cortopassi GA (2009) Inhibition of mitochondrial function induces an integrated stress response in oligodendroglia. *Neurobiol Dis* 34(2): 357–365.
31. Earle WR (1943) Production of malignancy *in vitro*. IV The mouse fibroblast cultures and changes seen in living cells. *J Natl Cancer Inst* 4:165–212.
32. Ishikawa K, et al. (2008) ROS-generating mitochondrial DNA mutations can regulate tumor cell metastasis. *Science* 320(5876):661–664.
33. Hashizume O, et al. (2012) Specific mitochondrial DNA mutation in mice regulates diabetes and lymphoma development. *Proc Natl Acad Sci USA* 109(26):10528–10533.
34. Fan W, Lin CS, Potluri P, Procaccio V, Wallace DC (2012) mtDNA lineage analysis of mouse L-cell lines reveals the accumulation of multiple mtDNA mutants and intermolecular recombination. *Genes Dev* 26(4):384–394.
35. Salomão SR, et al. (2004) Visual electrophysiologic findings in patients from an extensive Brazilian family with Leber's hereditary optic neuropathy. *Doc Ophthalmol* 108(2):147–155.
36. Shibata K, Shibagaki Y, Nagai C, Iwata M (1999) Visual evoked potentials and electroretinograms in an early stage of Leber's hereditary optic neuropathy. *J Neurol* 246 (9):847–849.
37. Carelli V, Ross-Cisneros FN, Sadun AA (2004) Mitochondrial dysfunction as a cause of optic neuropathies. *Prog Retin Eye Res* 23(1):53–89.
38. Sadun AA, Win PH, Ross-Cisneros FN, Walker SO, Carelli V (2000) Leber's hereditary optic neuropathy differentially affects smaller axons in the optic nerve. *Trans Am Ophthalmol Soc* 98:223–232, discussion 232–235.
39. Brand MD (2010) The sites and topology of mitochondrial superoxide production. *Exp Gerontol* 45(7-8):466–472.
40. Pryde KR, Hirst J (2011) Superoxide is produced by the reduced flavin in mitochondrial complex I: A single, unified mechanism that applies during both forward and reverse electron transfer. *J Biol Chem* 286(20):18056–18065.
41. Wong A, Cortopassi G (1997) mtDNA mutations confer cellular sensitivity to oxidant stress that is partially rescued by calcium depletion and cyclosporin A. *Biochem Biophys Res Commun* 239(1):139–145.
42. Porcelli AM, et al. (2009) Respiratory complex I dysfunction due to mitochondrial DNA mutations shifts the voltage threshold for opening of the permeability transition pore toward resting levels. *J Biol Chem* 284(4):2045–2052.
43. Schriner SE, et al. (2005) Extension of murine life span by overexpression of catalase targeted to mitochondria. *Science* 308(5730):1909–1911.
44. Melov S, et al. (1998) A novel neurological phenotype in mice lacking mitochondrial manganese superoxide dismutase. *Nat Genet* 18(2):159–163.
45. Melov S, et al. (2001) Lifespan extension and rescue of spongiform encephalopathy in superoxide dismutase 2 nullizygous mice treated with superoxide dismutase-catalase mimetics. *J Neurosci* 21(21):8348–8353.
46. Bayona-Bafaluy MP, Manfredi G, Moraes CT (2003) A chemical enucleation method for the transfer of mitochondrial DNA to rho(o) cells. *Nucleic Acids Res* 31(16):e98.
47. Trounce I, Wallace DC (1996) Production of transmitochondrial mouse cell lines by cybrid rescue of rhodamine-6G pre-treated L-cells. *Somat Cell Mol Genet* 22(1):81–85.
48. Nagy A, Gertsenstein M, Vinterson K, Behringer R (2003) *Manipulating the Mouse Embryo, a Laboratory Manual* (Cold Spring Harbor Laboratory Press, Cold Spring Harbor, NY), 3rd Ed.